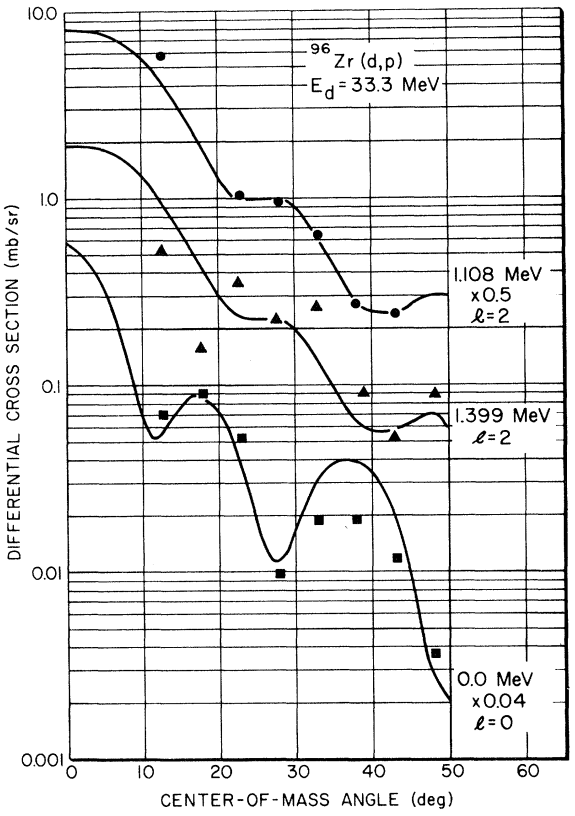

FIG. 11. Experimental angular distributions for $l=0$ and $l=2$ levels in ^{96}Zr(d,p) (points) in comparison with distorted-wave calculations (smooth curves).

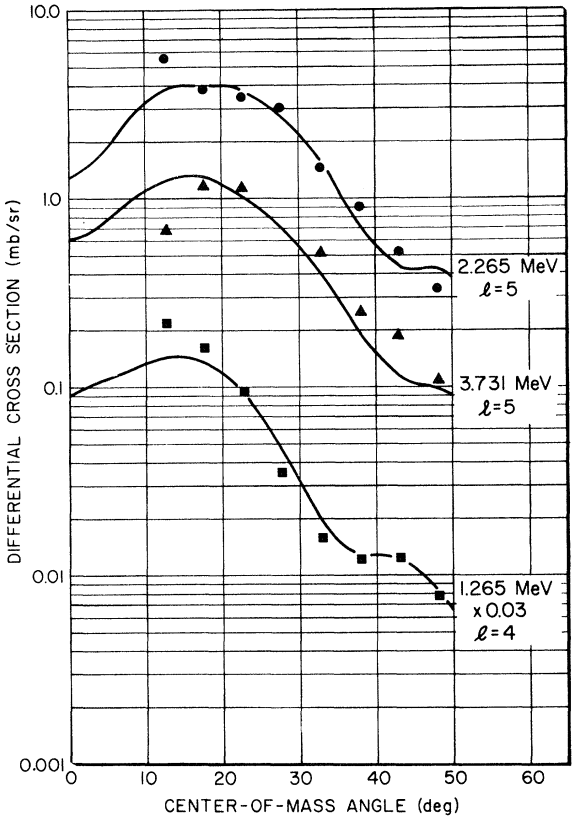

FIG. 12. Experimental angular distributions for $l=4$ and $l=5$ transitions in ^{96}Zr(d,p) (points) in comparison with distorted-wave calculations (smooth curves).

the small isotopic abundance of the target and hence the results are only approximations to the complete picture.

The spectroscopic strengths for the $2d_{5/2}$, $3s_{1/2}$, and $1g_{7/2}$ states agree well with the expected values. The measured spectroscopic strength for the $2d_{3/2}$ states is somewhat higher than expected and that for $1h_{11/2}$ states is ~50–60% of that expected. Similar results were reported previously for ^{91}Zr and ^{92}Zr.[8]

ACKNOWLEDGMENTS

We are indebted to M. L. Halbert and J. B. Ball for many valuable discussions and to M. L. Halbert for his assistance in taking the data. The careful plate scanning of Phyllis Wagner and Barbara Monroe is gratefully acknowledged.

---

*Research supported by the Army Research Office – Durham under a grant to The University of Tennessee and by U. S. Atomic Energy Commission under contract with Union Carbide Corporation.

†Present address: Air Force Weapons Laboratory, Kirtland Air Force Base, Albuquerque, New Mexico 87117.

[1]C. R. Bingham, M. L. Halbert, and R. H. Bassel, Phys. Rev. 148, 1174 (1966).

[2]B. L. Cohen and O. V. Chubinsky, Phys. Rev. 131, 2184 (1963).

[3]C. E. Brient, E. L. Hudspeth, E. M. Bernstein, and W. R. Smith, Phys. Rev. 148, 1221 (1966).

[4]R. L. Preston, H. J. Martin, and M. B. Sampson, Phys. Rev. 121, 1741 (1961).

[5]J. K. Dickens and E. Eichler, Nucl. Phys. A101, 408 (1967).

[6]J. S. Forster, L. L. Green, N. W. Henderson, J. L. Hutton, G. D. Jones, J. F. Sharpey-Schafer, A. G. Craig, and G. A. Stephens, Nucl. Phys. A101, 113 (1967).

[7]G. Simmerstad, M. Iverson, and J. J. Kraushaar, Technical Progress Report, University of Colorado Nu-

clear Physics Laboratory, Report No. Coo-535-603, 1969 (unpublished).
[8]C. R. Bingham and M. L. Halbert, Phys. Rev. C 2, 2297 (1970).
[9]N. Baron, C. L. Fink, P. R. Christensen, J. Nickles, and T. Torsteinsen, Bull. Am. Phys. Soc. 17, 50 (1972).
[10]E. Newman, L. C. Becker, B. M. Preedom, and J. C. Hiebert, Nucl. Phys. A100, 225 (1967).
[11]M. P. Fricke, E. E. Gross, B. J. Morton, and A. Zucker, Phys. Rev. 156, 1207 (1967).
[12]W. Whaling, in *Handbuch der Physik*, edited by S. Flügge (Springer-Verlag, Berlin, Germany, 1958), Vol. 34, pp. 193-217.
[13]Program developed by R. M. Drisko, R. H. Bassel, and G. R. Satchler.
[14]G. R. Satchler, private communication.
[15]C. R. Bingham and M. L. Halbert, Phys. Rev. 158, 1085 (1967).
[16]F. G. Perey and A. M. Saruis, Nucl. Phys. 70, 225 (1965).
[17]J. K. Dickens, R. M. Drisko, F. G. Perey, and G. R. Satchler, Phys. Letters 15, 337 (1965).
[18]C. R. Bingham, M. L. Halbert, and A. R. Quinton, Phys. Rev. 180, 1197 (1969).
[19]I. Talmi, Phys. Rev. 126, 2116 (1962).
[20]J. B. Ball and C. B. Fulmer, Phys. Rev. 172, 1199 (1968).

PHYSICAL REVIEW C VOLUME 7, NUMBER 4 APRIL 1973

Asymmetry in Nuclear Fission

M. G. Mustafa*
Oak Ridge National Laboratory,† Oak Ridge, Tennessee 37830

and

U. Mosel‡
University of Washington,§ Department of Physics, Seattle, Washington 98195, and Oak Ridge National Laboratory, Oak Ridge, Tennessee 37830

and

H. W. Schmitt
Oak Ridge National Laboratory, Oak Ridge, Tennessee 37830
(Received 8 September 1972)

The two-center shell model for fission has been generalized to include asymmetric deformations. The calculation of the potential energy involves four independent shape variables, where only two were required in the symmetric calculations. Potential energy calculations have been carried out for ^{202}Pb, ^{210}Po, ^{236}U, ^{248}Cm, ^{252}Fm, ^{258}Fm, and ^{264}Fm. Asymmetric fission is found to be energetically preferred in ^{236}U, ^{248}Cm, and ^{252}Fm; and symmetric fission is preferred in ^{202}Pb, ^{210}Po, ^{258}Fm, and ^{264}Fm. Two of these nuclei, namely ^{236}U and ^{210}Po, have been studied in detail. It is seen that the asymmetry in ^{236}U remains almost constant from the second saddle to scission, whereas in ^{210}Po (and also in ^{202}Pb), the preferred shape changes from asymmetry in the region of the second saddle to symmetry in the region of scission. The results for Fm isotopes indicate that there is a transition from asymmetric fission in the lighter Fm isotopes to symmetric fission in the heavier Fm isotopes. The preference for symmetric mass division in ^{264}Fm is very strong, since two double-magic $^{132}_{50}Sn_{82}$ fragments are formed at symmetry. In general, the structures which appear in the potential energy surfaces are the results of an interplay between compound-nucleus shell structure, fragment shell structures, and liquid-drop-model energies. Comparisons of our results with experimental observations indicate that the observed mass distribution is correlated with the potential energy surface in the neighborhood of scission.

I. INTRODUCTION

The most significant achievement in the calculation of potential energy surfaces for nuclear fission and heavy-ion reactions in recent years has been the development of methods for calculating shell corrections to smooth liquid-drop-model surfaces.[1] These methods allow one to calculate potential energy surfaces[2,3] rather quantitatively, and thus help one to understand nuclear fission and fusion in a more detailed way.

In particular, it has been a long-standing hope that such potential energy calculations would perhaps provide a basis for the observed dominance

of asymmetric mass divisions in low-energy fission of the actinides. Although this mass asymmetry has long been considered to be a consequence of shell effects, it is only recently that theoretical calculations, by Möller and Nilsson,[4] indeed established an instability of the second barrier to asymmetric deformations. It is our aim in this paper to show the physical reason for this instability and to show its connection with specific fragment structure properties.

Since all calculations based on extended Nilsson models, i.e., one-center single-particle potentials, are not suitable for an investigation of this problem, we have undertaken a systematic study of potential energy surfaces for nuclear fission by generalizing the two-center shell model[3,5] to asymmetric deformations.[6] Since this generalized two-center model can describe the correct shell structure of a fissioning nucleus as well as that of two noninteracting, well separated nuclei, it is very suitable for an investigation of the fission problem. In the next section we will, therefore, present the mathematical details of the model and discuss some of its properties. In subsequent sections we will systematically investigate the dependence of the nuclear potential energy on asymmetric deformations and the connection between the topology of the potential energy surface and the structure of the nascent fragments.

II. ASYMMETRIC TWO-CENTER MODEL

The Hamiltonian used for the calculation of single-particle energies appropriate for highly deformed, and even separated nuclear shapes, as they appear in nuclear fission and heavy-ion interactions, is that of the asymmetric two-center model. Since earlier versions of this model either violated nuclear saturation properties[7] or were too schematic for a detailed quantitative investigation of fission potential energy surfaces,[8] we introduce a new generalization of the symmetric two-center model to asymmetric shapes, which avoids these difficulties.[9]

We make the following ansatz for the single-particle Hamiltonian:

$$H = T + \tfrac{1}{2} m\,\omega_{\rho i}{}^2(z)\rho^2 + \tfrac{1}{2} m\,\omega_{zi}{}^2(z - z_i)^2 + V_{\rm corr} + V(\vec{l}, \vec{s}) \tag{1}$$

with $i = 1$ for $z > 0$ and $i = 2$ for $z > 0$. The nuclear shapes that can be described by this model are essentially those of two nonidentical semispheroids connected by a smooth neck. The centers of the semispheriods are located at z_1 and z_2. The smoothing of the neck is achieved, in direct generalization of the corresponding expression in symmetric calculations,[3] by choosing:

$$V_{\rm corr} = \tfrac{1}{2} m\,\omega_{zi}{}^2 \xi_i (z - z_i)^4 \theta(|z| - |z_i|), \tag{2}$$

where $\theta(x) = 0$ for $x > 0$ and $\theta(x) = 1$ for $x < 0$.

It should be mentioned here that this potential (or shape) parametrization is suitable both for the description of heavy-ion interactions and of nuclear fission. In the former process the two ions approach each other only slightly distorted compared with the fission fragment deformations. This case is contained in the present parametrization by setting $\xi_i = 0$. The shapes describable by the potential are then those of two unequal separated or overlapping spheroids, i.e., those appearing before and about the contact point in heavy-ion reactions.

The function $\omega_{\rho i}(z)$ in Eq. (1) is chosen to depend on z in the same way as the purely z-dependent part of the potential:

$$\omega_{\rho i}{}^2(z) = \mathring{\omega}_{\rho i}{}^2 + \alpha_i[(z - z_i)^2 + \xi_i (z - z_i)^4]\,\theta(|z| - |z_i|), \tag{3}$$

The quantities $\mathring{\omega}_{\rho i}$, α_i, ξ_i are defined in Appendix A. $\mathring{\omega}_{\rho 1}$ and $\mathring{\omega}_{\rho 2}$ are inversely proportional to the

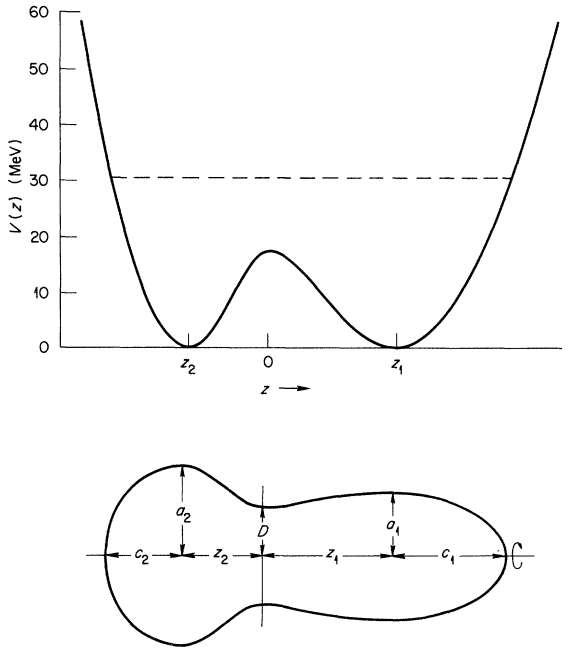

FIG. 1. The lower portion of the figure shows a nuclear shape described by the Hamiltonian given in Eq. (1); the upper portion shows the corresponding z-dependent part of the single-particle potential and is given by $V(z) = \frac{1}{2} m\omega_{zi}{}^2(z - z_i)^2 + m\omega_{zi}{}^2 \xi_i (z - z_i)^4 \theta(|z| - |z_i|)$ with $i = 1$ for $z > 0$ and $i = 2$ for $z < 0$ (see Sec. II and Appendix A). It is to be noted that this potential is independent of the transverse semiaxes a_1 and a_2.

transverse semiaxes a_1 and a_2 (see Fig. 1), and α_i and ξ_i are chosen to allow a smooth transition from $\mathring{\omega}_{\rho 1}$ to $\mathring{\omega}_{\rho 2}$.

The nuclear shape corresponding to the single-particle potential $V(\rho, z)$ in Eq. (1) is obtained in the usual way by assuming that the nuclear surface follows an equipotential surface with the value V_0:

$$V(\rho, z) = V_0, \quad \rho = \rho(z). \tag{4}$$

For the potential value V_0 we take, as usual, $V_0 = \frac{1}{2} m \omega_0^2 R^2$ with R being the nuclear radius and ω_0 the oscillator frequency given by $\hbar\omega_0 = 41 A^{-1/3}$ MeV, where A is the nuclear mass number. The shape parameters can then be determined from various conditions for smooth transitions of the potential and its derivatives at $z=0$, volume conservation, and the condition that for large separations (large $z_1 - z_2$) two independent Nilsson potentials should be contained in the present parametrization. (For details of these conditions see Appendix A). These requirements finally lead to four independent shape parameters for which we choose the neck radius D (in fermis), the volume ratio of the fragments λ, and the two additional coordinates α (describing the relative maximum ρ dimensions of the fragments) and σ (describing the elongation of one of the two fragments). The exact definitions for these quantities are given in Appendix A. (See also Fig. 1).

The angular momentum-dependent term $V(\vec{l}, \vec{s})$ is taken to be:

$$V(\vec{l}, \vec{s}) = \begin{cases} C(z_1)\vec{l}_1 \cdot \vec{s} + D(z_1)(\vec{l}_1^{\,2} - \langle \vec{l}_1^{\,2} \rangle), \\ C(z_2)\vec{l}_2 \cdot \vec{s} + D(z_2)(\vec{l}_2^{\,2} - \langle \vec{l}_2^{\,2} \rangle), \end{cases} \tag{5}$$

where $\vec{l}_1$ and $\vec{l}_2$ are the pseudoangular momenta with respect to the two centers at z_1 and z_2. These pseudoangular momenta are defined in terms of the stretched coordinates appropriate to each of the two half spheroids.[3] In order to assure a correct transition to the appropriate C and D values for the fragment regions, we have introduced the Nilsson parameters κ and μ in the following way:

$$\begin{aligned} C(z_i) &= -2\hbar\bar{\omega}(z_i)\kappa(z_i), \\ D(z_i) &= \tfrac{1}{2} C(z_i)\mu(z_i), \end{aligned} \tag{6}$$

where $\bar{\omega}$ is defined by:

$$\bar{\omega}(z_i) = (\omega_{zi} \cdot \mathring{\omega}_{\rho i}^{\,2})^{1/3}. \tag{7}$$

This assures a continuous transition from the oscillator constant for the fissioning nucleus to the two different oscillator constants for the final fragments. The quantities $\kappa(z_i)$ and $\mu(z_i)$ are interpolated linearly between the values for the compound and the fragment regions. The interpolation variable is $\bar{\omega}$. The values of κ and μ are given in Table I and are based on the values of Nilsson *et al.*[2] and Arseniev, Sobiczewski, and Soloviev.[10]

The Hamiltonian (1) is then diagonalized in a basis consisting of eigenstates of the basis Hamiltonian:

$$H_0 = T + \tfrac{1}{2} m \bar{\omega}_\rho^{\,2}\rho^2 + \tfrac{1}{2} m \omega_{zi}^{\,2}(z - z_i)^2. \tag{8}$$

Here $\bar{\omega}_\rho$ is the arithmetic average of $\omega_{\rho 1}$ and $\omega_{\rho 2}$. The basis functions of H_0 can be obtained by a simple matching procedure.[5] This basis choice, compared with the standard deformed harmonic-oscillator basis used by most other groups, has the advantage that it already contains the over-all deformation of the nuclear shape, even at scission and beyond. This means that the most important deformation-dependent terms in the Hamiltonian are already diagonal and only small perturbations have to be diagonalized; thus good convergence is assured.

In contrast, we note that the one-center deformed harmonic-oscillator basis leads to a progressively worse convergence when applied to the description of shapes at the scission configuration and beyond. This precludes any description of heavy-ion interactions and of the latter stages of fission in which such configurations occur. The two-center basis states have none of these shortcomings, and the convergence even improves with increasing separation.

This basis choice also leads to a natural generalization of the term $\langle \vec{l}_i^{\,2} \rangle$ which in the standard Nilsson model is given by[11] $N(N+3)/2$. Here N is the principal oscillator quantum number. Since the eigenenergies of H_0 are given by[5]

$$E_0 = (N_\rho + 1)\hbar\bar{\omega}_\rho + (n_{zi} + \tfrac{1}{2})\hbar\omega_{zi} \tag{9}$$

with n_{zi} being an integer only in the cases of either

TABLE I. The table lists the single-particle parameters κ and μ for protons and neutrons for the two compound-nucleus regions discussed in the text and for the fragment regions. They are, except for very small changes, taken from Nilsson *et al.* (Ref. 2) for the two compound-nucleus regions and from Arseniev, Sobiczewski, and Soloviev (Ref. 10) for the fragment regions.

	Protons		Neutrons	
Mass region	κ	μ	κ	μ
$A \approx 100$	0.0688	0.558	0.0638	0.491
$A \approx 132$	0.0671	0.572	0.0638	0.493
$A \approx 200$	0.0610	0.626	0.0636	0.370
$A \approx 250$	0.0580	0.645	0.0635	0.330

zero or very large separations, we set

$$\langle \vec{I}_i^{\,2} \rangle = \tfrac{1}{2}(N_\rho + n_{zi})(N_\rho + n_{zi} + 3), \tag{10}$$

thus assuring the correct transition of this term from its proper value in the fissioning nucleus to that in the two fragments (see, e.g., Fig. 2 of Ref. 8).

The actual diagonalization of (1) has been performed in the basis mentioned above. We found that taking the 300 lowest eigenstates of H_0 (instead of using a specified number of shells) at each deformation assures good convergence – better than 10 keV in the shell corrections.

The choice of oscillator potentials in (1) is not a necessary choice, since the two-center model can be formulated with other potentials as well, e.g., Woods-Saxon potentials. It has been claimed, especially by Bolsterli *et al.*,[2] that the harmonic-oscillator potential is inferior to the more realistic finite depth potentials. This claim, although correct for the description of many physical phenomena (e.g., single-particle reactions), is misleading in the present context. First, the asymptotic behavior of bound-state wave functions, which is different in the two models, nowhere enters into the calculation of potential energy surfaces. Second, the seemingly obvious advantage of using a more realistic finite depth potential is lost because the Strutinsky shell correction method requires the presence of single-particle states rather high (≈20 MeV) above the Fermi surface. This necessitates the discretization of the continuum into physically meaningless single-particle states that appear as a byproduct in diagonalization of the finite depth potentials in oscillator basis functions. In other words, the use of the Strutinsky shell correction method necessitates, in effect, the introduction of infinitely high potential walls outside the nuclear radius, even in the case of "finite depth" potentials. Thus, the only remaining advantage in the use of finite depth potentials is the better description of the surface region, which makes the use of the $\vec{l}^2$ term unnecessary.

After having obtained the single-particle energies of (1) as described above, shell corections δU are generated from these by using the Strutinsky prescription[1] with a smearing width of $1.2\hbar\omega$ and a correction polynomial of sixth order.

The liquid-drop model has been calculated for the shapes given by Eq. (4) with the parameters used by Myers and Swiatecki,[1] except that the surface symmetry coefficient κ_s has been changed to the value given by Seeger.[12] This change was suggested by Johansson, Nilsson, and Szymanski[13] who obtained second barriers which were systematically too high in the actinide region when the original Myers and Swiatecki value was used. A similar value of κ_s has also been suggested by Pauli and Ledergerber.[2] The most realistic value for κ_s, of course, can only be obtained in a simultaneous refit of the liquid-drop-model plus shell

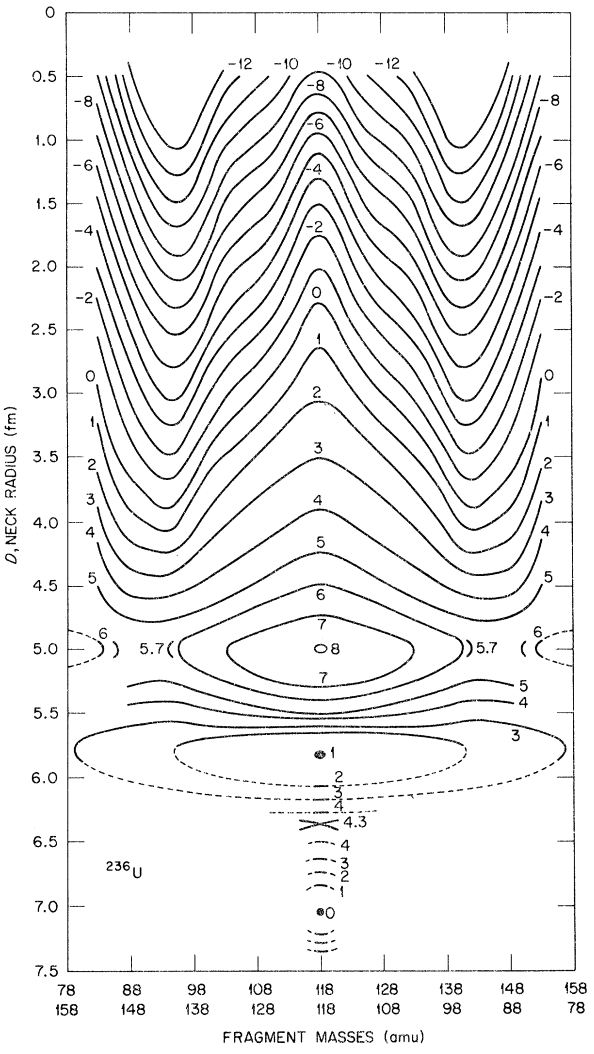

FIG. 2. The two-dimensional potential energy surface $V(\lambda,D)$ for ^{236}U is shown; λ is the volume (mass) ratio of the portions of the nucleus on either side of the neck plane, and D is the radius of the neck in fermis. The energy has been minimized with respect to α and σ, which are the other two shape parameters describing the asymmetric nuclear shape (see Appendix A). The zero reference energy is at the ground state of ^{236}U. The numbers labeling the contour lines give the contour energies in MeV. The solid lines are the results of our calculations; the dashed lines have not been calculated, but are included as approximate curves for the completeness of the $V(\lambda,D)$ plot.

corrections to experimental masses, a calculation not yet undertaken. The results for mass asymmetry in fission and the indications of fragment shell structure effects in the potential energy surfaces that we shall present in this paper are not sensitively dependent on κ_s. The quantity κ_s is, however, more critical in detailed calculations of barrier heights.

The pairing interaction has been taken into account in the BCS formalism using Z levels for the protons and N levels for the neutrons. The pairing strengths that give good fits to the odd-even mass difference in the heavy-element region are

$$G_p = \frac{19.4}{A}\ \text{MeV}, \quad G_n = \frac{13.8}{A}\ \text{MeV}, \tag{11}$$

and those in the $A \sim 200$ region are

$$\begin{aligned} G_p &= [20.8 - 0.0933(A-180)]/A\ \text{MeV}, \\ G_n &= [14.5 - 0.0233(A-180)]/A\ \text{MeV}. \end{aligned} \tag{12}$$

They are taken to be independent of deformation, since recent calculations in the range $180 \lesssim A \lesssim 212$ indicate that the assumption of a surface-dependent pairing strength is incompatible with experimental data on fission barriers in that mass region.[14] The pairing energy is then given by

$$E_p = \sum_{p,n}\left(2\sum_{\nu}\epsilon_\nu v_\nu^2 - 2\sum_{\nu}^{\nu_f}\epsilon_\nu - \frac{\Delta^2}{G}\right). \tag{13}$$

The total potential energy is given by

$$V = E_{\text{LDM}} + E_p + \delta U,$$

where E_{LDM} is the liquid-drop-model energy.

Our calculations have been carried out by fixing successive values of D and λ, and then performing for each of these a two-dimensional potential energy surface calculation. By thus doing a full four-dimensional calculation, a correct determination of the saddle-point location within the chosen shape parametrization is assured.[15]

III. RESULTS

Potential energies have been calculated for the following fissioning nuclei: ^{202}Pb, ^{210}Po, ^{236}U, ^{248}Cm, ^{252}Fm, ^{258}Fm, and ^{264}Fm. Two of these cases, namely ^{236}U and ^{210}Po, have been studied in detail.

Our procedure for carrying out the calculations, in general, was to fix values of the volume (or mass) ratio λ and the neck thickness D, and then to minimize the potential energy with respect to α and σ. We thereby obtain a matrix of values $V(\lambda, D)$, for a given fissioning nucleus. The elimination of the two other shape parameters by minimization is not meant to imply that the fissioning system always follows the minimum energy path; rather, this procedure just permits the display of our results in terms of the two most important fission variables λ and D. The quantity D may serve as an approximate fission coordinate in the region beyond the second saddle point, where the

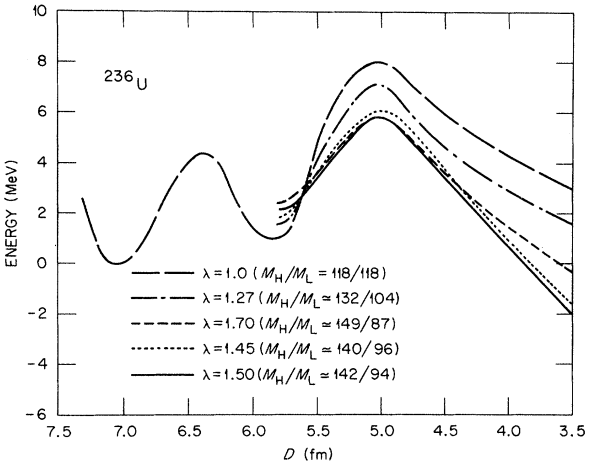

FIG. 3. The potential energy $V(D)$ as a function of neck thickness is shown for selected values of λ, for ^{236}U. These curves represent selected vertical cuts through Fig. 2. The energy has been minimized with respect to α and σ, and normalized to zero at the ground state. Note the rather sudden change from symmetric to asymmetric shapes at $D \cong 5.6$ fm.

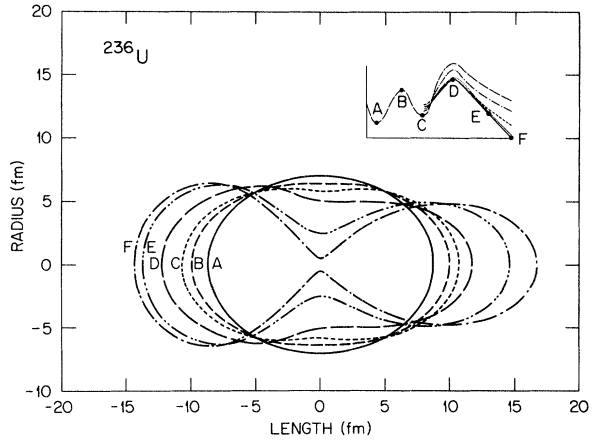

FIG. 4. Shapes of the ^{236}U nucleus at various points along the minimum potential energy path. The shapes labeled A, B, and C are reflection symmetric ($\lambda = 1$) and correspond to the neck radius 7.05 fm (approximate ground state), 6.4 fm (first saddle), and 5.8 fm (second minimum), respectively. The shapes labeled D, E, and F are asymmetric and correspond to neck radius and volume ratio of 5.0 fm, 1.5 (second saddle), 2.5 fm, 1.45, and 0.5 fm, 1.45, respectively.

constriction degree of freedom becomes important.[3]

A. $^{236}_{92}U_{144}$

The two-dimensional potential energy surface $V(\lambda, D)$ for ^{236}U is shown in Fig. 2. The ground state of this nucleus occurs at $D \cong 7.05$ fm, corresponding to a spheroidal shape.[16] Following the minimum potential path to scission we pass over the first barrier at $D \cong 6.4$ fm, for which the nuclear shape is reflection symmetric. Continuing into the second minimum at $D \cong 5.8$ fm, we find that a reflection-symmetric shape is still preferred, but that the potential becomes very soft towards asymmetric deformations. The minimum energy path crosses the second barrier at $D \cong 5.0$ fm with a quite asymmetric shape, namely $\lambda \cong 145/91$. Continuing towards scission, i.e., towards smaller D values, we see that the minimum in the potential energy surface shifts slightly, to $\lambda \cong 140/96$, in excellent agreement with the most probable mass division observed in the low-energy fission of ^{236}U.[17]

We note also, from this figure, that the asymmetric barrier is favored by about 2.3 MeV relative to the symmetric barrier, and that near scission the most probable asymmetric shapes are preferred by ~7 MeV relative to symmetry. The calculated barrier height (saddle-point energy) is in satisfactory agreement with the experimental value.[18]

In Fig. 3 we have plotted a few vertical cuts through Fig. 2. That is, we plot $V(D)$ for selected values of λ. The usual double hump in the barrier is apparent, and differences for different λ values are shown. This figure does not imply that the occurrence of a particular final λ at scission corresponds to a process that has followed one of these curves; rather, the system may move over the full four-dimensional potential surface, and any final λ may result from events, for example, which cross the saddle at $\lambda \cong 145/91$ (or any other λ), depending on the quantum dynamics of the process.

The shapes of the nucleus at various points along the minimum potential energy path are shown in Fig. 4. The shapes A, B, and C are reflection symmetric; shapes D, E, and F are asymmetric. It is interesting that near scission the heavy fragment appears to have a more nearly spherical shape than the light fragment.

In Fig. 5 we show a comparison of saddle-point shapes for different values of λ. The point to note here is that the shapes are not very different, and the nucleus does not have to change its shape very much to cover the full range of λ.

A similar, and perhaps more important comparison is shown in Fig. 6 for shapes nearer scission, at $D = 2.5$ fm. Again it is clear that the full range of λ is accessible with relatively small changes in shape.

Since the calculations of the full four-dimensional potential energy surfaces are very time consuming, our calculations for most other nuclei are restricted to cuts $V(\lambda)$ for different values of D around and beyond the second saddle point, as located within the symmetric calculations. To

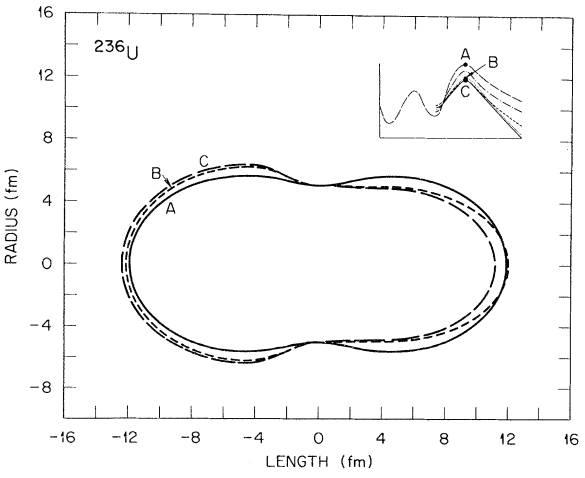

FIG. 5. Shapes of the ^{236}U nucleus for different values of λ are compared at $D = 5.0$ fm, corresponding to the second saddle region. The shapes A, B, and C correspond to $\lambda = 1.0$, 1.45, and 1.7, respectively.

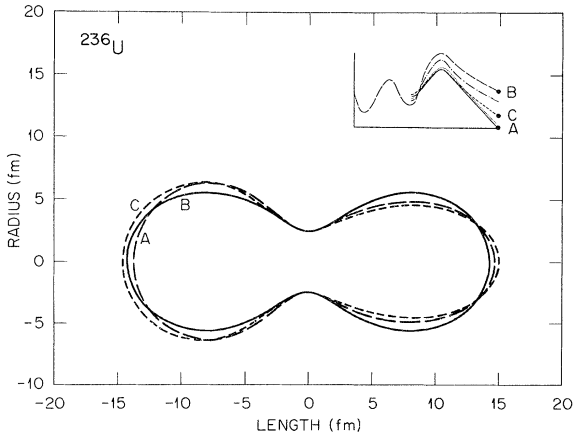

FIG. 6. Shapes of the ^{236}U nucleus for different values of λ are compared at $D = 2.5$ fm, corresponding to the approach to scission. The shapes A, B, and C correspond to $\lambda = 1.45$, 1.0, and 1.7, respectively.

illustrate the relationship between the full potential energy surface and these cuts we show in Fig. 7 the curves $V(\lambda)$ for ^{236}U. The curve corresponding to the neighborhood of the second saddle point is labeled $D = 5.0$. This curve gives a good indication of the behavior of the potential energy surface about the saddle, although it alone does not suffice to localize the saddle point unequivocally.

Similarly, a key indication of the behavior of the potential energy surface near scission is the function $V(\lambda)$ for $D = D_{\to sc}$, where $D_{\to sc}$ is some value of D approaching scission, chosen generally in the range 2 to 4 fm. Such a curve for ^{236}U is labeled $D = 2.5$ in Fig. 7.

The remaining curves in Fig. 7 correspond to $D = 5.7$, close to the second minimum in the potential energy surface, and to an intermediate point between $D = 5.0$ (saddle point) and $D = 2.5$, namely $D = 4.5$. It is seen in Fig. 7, as in Fig. 2, that asymmetric shapes ($\lambda \cong 145/91$) are favored at the saddle, and that the potential energy minimum shifts slightly, to $\lambda \cong 140/96$, as D decreases toward scission.

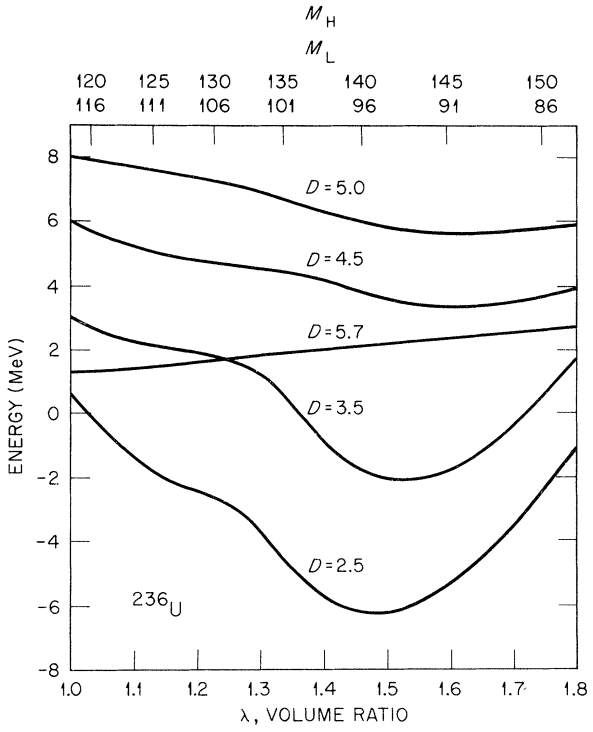

FIG. 7. The potential energy for ^{236}U as a function of λ, the volume ratio of the portions of the nucleus on either side of the neck plane, for several values of D, the radius of the neck in fermis. The energy has been minimized with respect to α and σ and normalized to zero for the ground-state energy.

Let us discuss one further aspect of the ^{236}U results. It has long been known that the Q values for fission, i.e., the available energy for fission into various fragment mass divisions, favor division into final fragments with $\lambda \cong 132/104$. The minimum potential energy near scission is seen here, however, to occur at $\lambda \cong 140/96$, in agreement with experiment. Our explanation for this may be stated approximately as follows: When λ is precisely (or very close to) 132/104, the double-magic mass-132 partner tends toward sphericity to take advantage of its large binding energy. In so doing, however, the repulsive Coulomb poten-

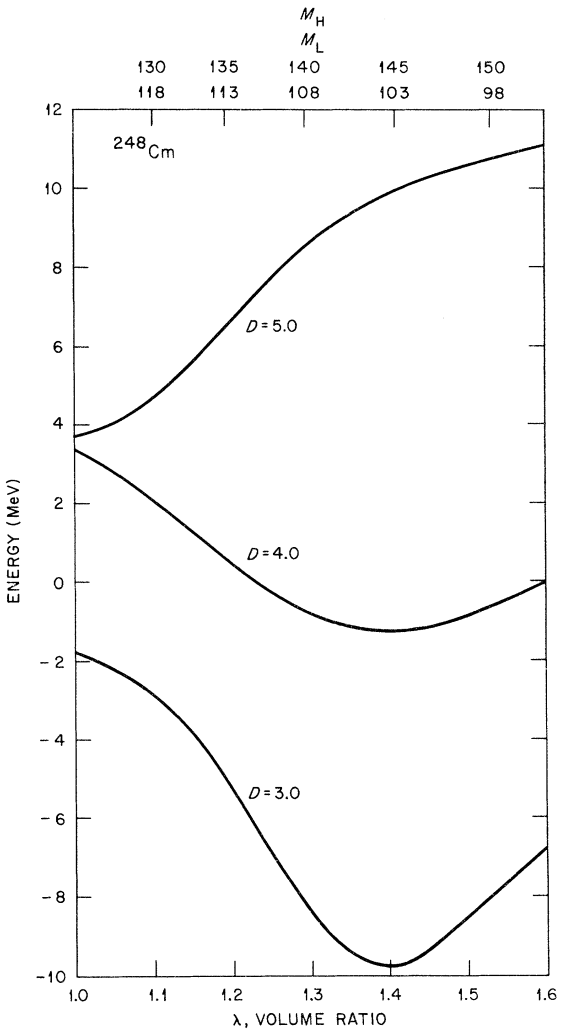

FIG. 8. The potential energy for ^{248}Cm as a function of λ, the volume ratio of the portions of the nucleus on either side of the neck plane, for several values of D, the radius of the neck in fermis. The energy has been minimized with respect to α and σ and normalized to zero for the ground-state energy.

tial tends toward higher values, so that the total potential energy is actually higher than that at $\lambda \cong 140/96$, where the additional ~8 nucleons in the heavy fragment apparently provide an optimum compromise between the increased binding energy of nuclei approaching double-magic configurations, and the reduced stiffnesses of nuclei receding from closed-shell configurations.

B. $^{248}_{96}Cm_{152}$

The potential energy for this nucleus has been studied by examining cuts in the $V(\lambda, D)$ surface, showing $V(\lambda)$ at $D = 5.0$, 4.0, and 3.0 fm. The results of these calculations are shown in Fig. 8.

The symmetric saddle point for this nucleus occurs at $4.0 \lesssim D \lesssim 5.0$ fm; the curve labeled $D = 5.0$ in Fig. 8 indicates that the preferred shape is reflection symmetric. As the system continues toward scission, we see that asymmetric shapes become preferred (see curve for $D = 4.0$) and this preference becomes even stronger at $D = 3.0$, as evidenced by the stronger minimum at $\lambda \cong 144/104$.

C. $^{252}_{100}Fm_{152}$, $^{258}_{100}Fm_{158}$, and $^{264}_{100}Fm_{164}$

The potential energies for these nuclei have been studied, as in the case of ^{248}Cm, by examining cuts through the $V(\lambda, D)$ surfaces, showing $V(\lambda)$ for several values of D. The results are shown in Figs. 9–11.

The saddle point in ^{252}Fm, from reflection-symmetric calculations,[3] occurs at about $D = 4.87$. The curve showing $V(\lambda)$ for $D = 4.87$ in Fig. 9 indicates that here the preferred shape is still reflection symmetric. Similar results are obtained for ^{258}Fm and ^{264}Fm, as shown by the curves labeled $D = 5.0$ in Figs. 10 and 11.

As D becomes smaller, in the descent towards scission, we find that the minimum potential energy in ^{252}Fm shifts rather quickly to an asymmetric shape (curve labeled $D = 4.4$ in Fig. 9). The asymmetric shape then appears to remain preferred through intermediate stages (curve labeled

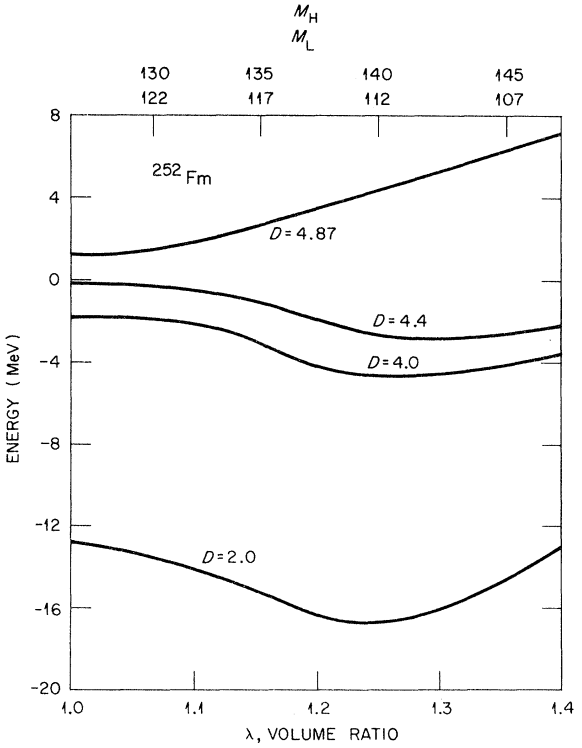

FIG. 9. The potential energy for ^{252}Fm as a function of λ, the volume ratio of the portions of the nucleus on either side of the neck plane, for several values of D, the radius of the neck in fermis. The energy has been minimized with respect to α and σ and normalized to zero for the ground-state energy.

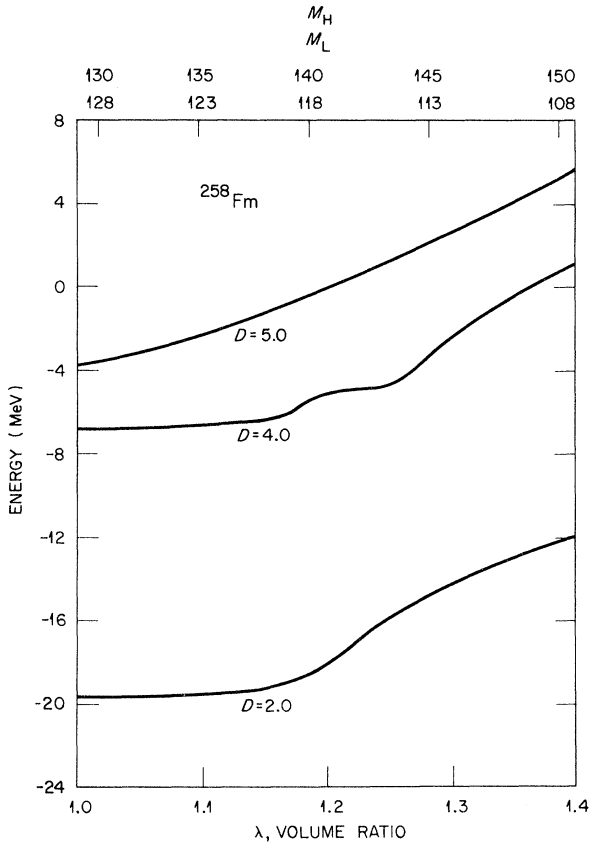

FIG. 10. The potential energy for ^{258}Fm as a function of λ, the volume ratio of the portions of the nucleus on either side of the neck plane, for several values of D, the radius of the neck in fermis. The energy has been minimized with respect to α and σ and normalized to zero for the ground-state energy.

$D = 4.0$) and onward towards scission (curve $D = 2.0$).

In contrast, the preferred shapes remain symmetric throughout the descent to scission for ^{258}Fm and ^{264}F, as seen in Figs. 10 and 11. The preference is quite strong, i.e., the potential minimum is quite sharp in ^{264}Fm, where symmetric fission results in the formation of two double-magic $^{132}_{50}Sn_{82}$ nuclei. The potential near scission in ^{258}Fm is softer towards asymmetry, exhibiting a somewhat flat shape as might be expected in the transition region between asymmetry (^{252}Fm) and symmetry (^{264}Fm).

Measurements of mass distributions in the fission of Fermium isotopes show asymmetric peaks in ^{254}Fm [19] and ^{256}Fm,[20] and a symmetric peak in ^{258}Fm.[21] The peak-to-valley ratio for ^{256}Fm is, however, only 12, a small value relative to the usual peak-to-valley ratios for the low-energy fission of actinides. A broader peak, with some dip in yield at symmetry has been found for ^{257}Fm.[21, 22] The results of our calculations are qualitatively in accord with the measurements. The most probable heavy-fragment mass for ^{252}Fm is calculated to be 140 amu, as observed for ^{254}Fm and ^{256}Fm. Although the rather flat potential calculated for ^{258}Fm would indicate a broader, more flat-topped mass distribution than is observed, there are two possible reasons why such a difference might occur; (1) The calculations are not refined sufficiently to give complete details

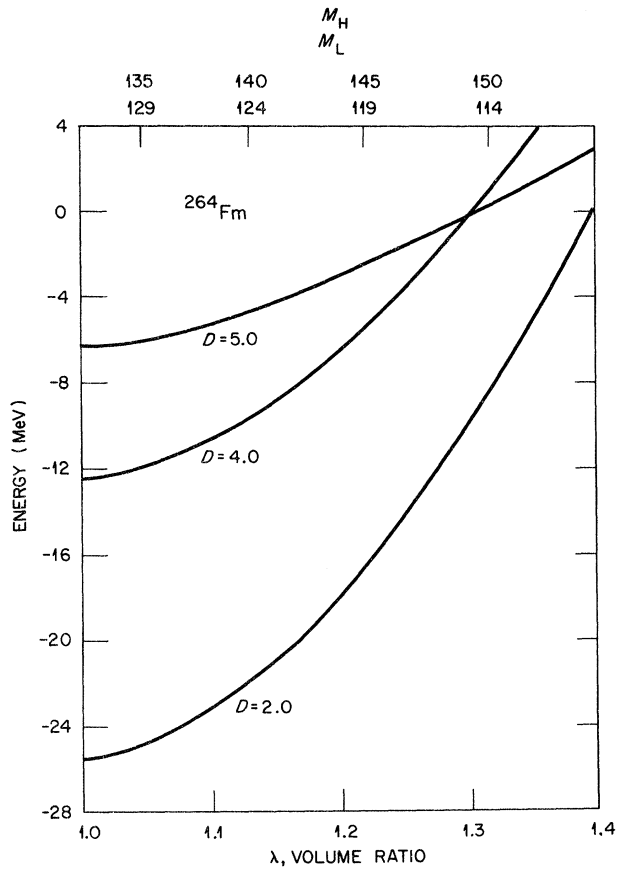

FIG. 11. The potential energy for ^{264}Fm as a function of λ, the volume ratio of the portions of the nucleus on either side of the neck plane, for several values of D, the radius of the neck in fermis. The energy has been minimized with respect to α and σ and normalized to zero for the ground-state energy.

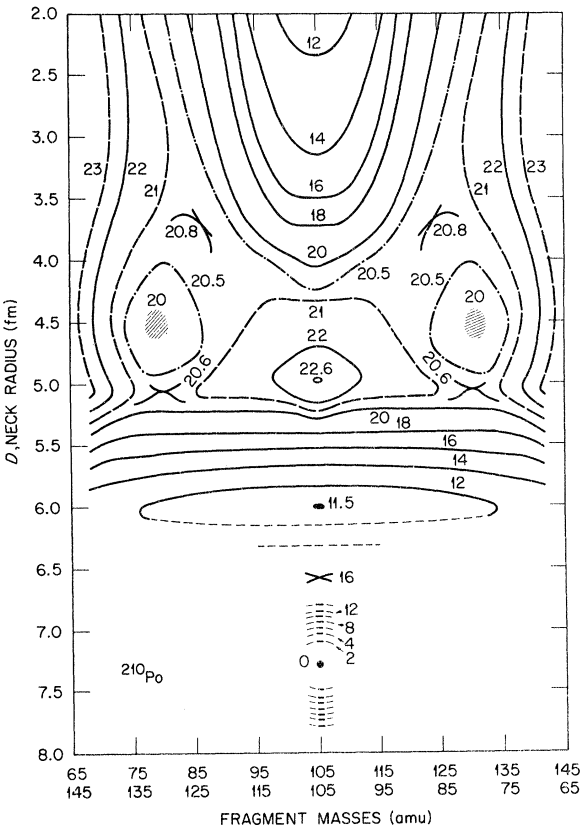

FIG. 12. The two-dimensional potential energy surface $V(\lambda,D)$ for ^{210}Po is shown; λ is the volume (mass) ratio of the portions of the nucleus on either side of the neck plane, and D is the radius of the neck in fermis. The energy has been minimized with respect to α and σ, which are the other two shape parameters describing the asymmetric nuclear shape (see Appendix A). The zero reference energy is at the ground state of ^{210}Po. The numbers labeling the contour lines give the contour energies in MeV. The heavy lines are the results of our calculations; the thin dashed lines have not been calculated, but are included as approximate curves for the completeness of the $V(\lambda,D)$ plot.

of the distributions, and there may be significant dynamic effects not yet taken into account, and (2) the measurements were made by bombarding ^{257}Fm with thermal neutrons, resulting in an excitation energy of ~6 MeV in the fissioning nucleus. The effect of increased excitation energy on the fargment mass distribution in this specific case is not known, but acts generally to enhance the symmetric yield. A measurement of the mass distribution for the spontaneous fission of ^{258}Fm, which is expected to be rather broad according to our calculations, would therefore be very important for a better understanding of this transition region.

The important point here is that a transition from asymmetric fission in the lighter Fm isotopes to symmetric fission in the heavier Fm isotopes occurs and is accounted for in the calculations of potential surfaces, in which fragment structure effects are evident. Specifically, symmetric fission becomes prominent when the number of neutrons reaches a value, apparently $N \sim 158$, at which two nearly-double-magic fragments can be formed.

D. $^{210}_{84}Po_{126}$

Some years ago, in the liquid-drop-model studies of Nix and Swiatecki,[23] it appeared that the liquid-drop model would successfully describe the fission of nuclei lighter than about radium. These nuclei, at medium excitation energies, generally produce fragment mass distributions peaked at symmetry, average total kinetic energies peaked at symmetry and slowly decreasing with asymmetry, and other observed quantities, all of whose general properties are consistent with results of the liquid-drop-model calculations.[23,24] (Measurements at low excitation energy do not exist.)

We have chosen the nucleus ^{210}Po to study in detail, as an example of nuclei lighter than radium, to determine whether the potential surface would exhibit an over-all liquid-drop character. A recent calculation of Bolsterli *et al.*[2] has indicated that the saddle point might occur at an asymmetric shape; if this were confirmed (as has, in fact, now occurred in our calculations, see below), the potential energy surface should show significant deviations from liquid-drop behavior.

The results of our potential energy calculations for ^{210}Po are shown in Fig. 12. The figure shows $V(\lambda, D)$, the potential having been minimized with respect to the other two shape variables α and σ, as for ^{236}U and all other nuclei. The ground state (zero energy) is at $D \cong 7.25$ fm; the first barrier is reflection symmetric and occurs at $D \cong 6.6$ fm, with $V = 16$ MeV. The second minimum occurs at $D \cong 6.0$ fm, with $V = 11.5$ MeV. Again, as in the case of ^{236}U, the second minimum is soft towards asymmetry and leads to a second saddle at an asymmetry of $\lambda \sim 130/80$. In this case the second saddle consists of a wide region from $D \sim 5.0$ to $D \sim 3.5$ in which the energy varies little (only ~1.8 MeV) and seems to show a slight dip at $D \sim 4.5$ fm. Beyond this saddle region the energetically favored path leads, via a steep valley, to symmetric mass division at scission.

The second saddle for this case is much higher than that for ^{236}U and agrees well with the experimental barrier height.[25] We note that the asymmetric saddle is favored by 2 MeV with respect to the symmetric barrier. The second minimum is quite narrow and lies at an excitation energy which is high relative to the ground state; an interesting question is whether this minimum can support an excited state whose wave function is concentrated in this region.

It is clear that the potential surface $V(\lambda, D)$ shown in Fig.12 contains prominent structures resulting from shell corrections and deviates appreciably from the smooth liquid-drop-like potential. Still, looking at the region of the surface for $D \lesssim 3.0$ fm, we see a resemblance to the smooth liquid-drop potential; we may understand on this basis, perhaps, why the liquid-drop-

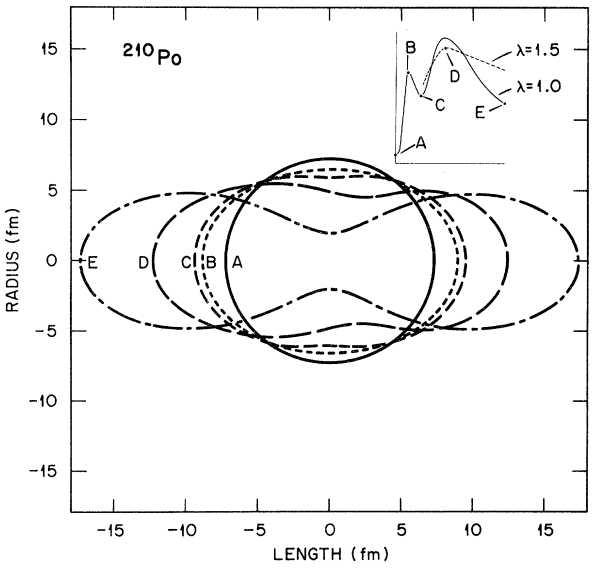

FIG. 13. The shape of the ^{210}Po nucleus at various points along the minimum energy path. The shapes labeled A, B, C, and E, are reflection symmetric ($\lambda = 1$) and correspond to neck radius 7.25 fm (ground state), 6.6 fm (first saddle), 6.0 fm (second minimum), and 2.0 fm (near scission), respectively. The shape labeled D is the asymmetric saddle shape and corresponds to the neck radius of 4.5 fm and volume ratio of 1.5.

model calculations initially appeared to be so successful.

In Fig. 13 we show the shapes of the $^{210}_{84}$Po nucleus at several points along the minimum potential energy path to scission. We note especially the asymmetric saddle shape, curve labeled D, and the quite elongated symmetric shape near scission, reflecting the fact that the nascent fragments ($^{105}_{42}$Mo at symmetry) are soft, mid-shell nuclei.

A plot of $V(\lambda)$ for several values of D is shown in Fig. 14. The curve labeled $D = 6.0$ corresponds to the second minimum, that labeled $D = 5.0$ corresponds to the onset of the second saddle. For $D \lesssim 4.0$ symmetric shapes are clearly preferred. This, as explained in the section on ^{236}U, is the kind of display we use in those cases where the entire $V(\lambda, D)$ surface has not been calculated; this figure provides a direct comparison of ^{210}Po with those cases.

Returning briefly to the calculated asymmetric saddle in ^{210}Po, we offer the following qualitative explanation for this phenomenon. The minimum in $V(\lambda)$ at the saddle point, where $D = 4.5 - 4.0$ fm, occurs at $\lambda \cong 1.7 \cong 132/78$ (see Fig. 14). This minimum and the shoulder which persists at this value of λ for cuts taken closer to scission, at $D = 3.5$, 3.0, and 2.0 fm, is probably due to the influence of the double-magic $^{132}_{50}Sn_{82}$ configuration reaching into the potential energy surface. Its strength is not enough to overcome the very strong liquid-drop-model preference for symmetry near scission, but is sufficient to cause the asymmetric minimum in the otherwise flat saddle region.

E. $^{202}_{82}Pb_{120}$

This nucleus is another example of nuclei lighter than radium, for which the fragment mass distributions are peaked at symmetry. We have examined a few slices $V(\lambda)$ at fixed D values, to ascertain whether the same general features occur in the $V(\lambda, D)$ surface for this nucleus as for ^{210}Po. The results are shown in Fig. 15.

The curve labeled $D = 4.37$ shows $V(\lambda)$ in the region of the saddle point, located on the basis

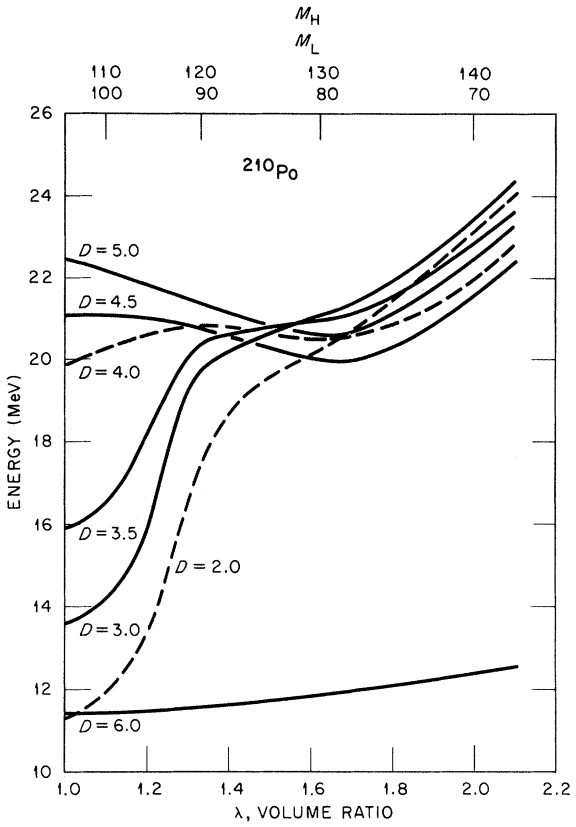

FIG. 14. The potential energy for ^{210}Po as a function of λ, the volume ratio of the portions of the nucleus on either side of the neck plane, for several values of D, the radius of the neck in fermis. The energy has been minimized with respect to α and σ and normalized to zero for the ground-state energy.

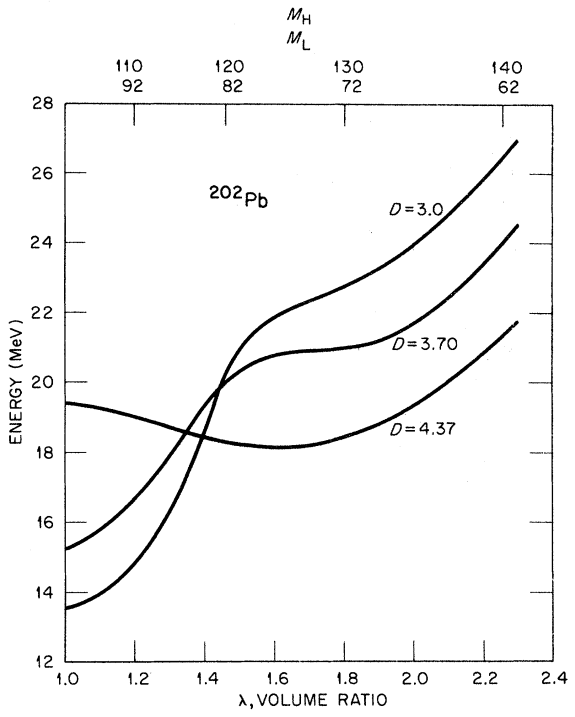

FIG. 15. The potential energy for ^{202}Pb as a function of λ, the volume ratio of the portions of the nucleus on either side of the neck plane, for several values of D, the radius of the neck in fermis. The energy has been minimized with respect to α and σ and normalized to zero for the ground-state energy.

of earlier calculations for reflection-symmetric shapes.[3] We see that, as in ^{210}Po, an asymmetric shape is preferred. The descent towards scission, i.e., $V(\lambda)$ at smaller values of D, indicates again a steep valley whose minimum is at symmetry.

Thus the results for ^{202}Pb seem to be qualitatively similar to those for ^{210}Po. In both cases the potential energy calculations indicate a mass distribution peaked at symmetry, in agreement with experimental observations for light nuclei.

IV. DISCUSSION AND SUMMARY

The comparison of our results with experiment, as discussed above, shows clearly that the observed mass distribution is correlated with the potential energy surface in the neighborhood of scission. In this region of the potential surface, fragment structure effects are identifiable and are strongly felt, as we have also shown. We, therefore, conclude that the observed mass distributions in low-energy nuclear fission are strongly influenced by specific fragment shell structures.

It is a remarkable coincidence that in ^{236}U, and possibly also in other actinides, the asymmetry remains almost constant from the saddle point to scission, whereas in ^{210}Po the preferred asymmetry changes drastically between saddle and scission. This comparison appears to us to illustrate the interesting interplay between the shells of the fissioning nucleus and those of the nascent fragments in the structure of the potential energy surfaces. The details of this interplay and the specific manner in which it occurs in the potential surface depends to some extent on the form of the single-particle potential and on the increase in height of the intermediate peak in $V(z)$ at the neck plane as the neck radius decreases toward scission. The analytical form we have used (see Sec. II) appears to be physically reasonable, but this aspect should ultimately be studied by means of self-consistent calculations.

Because of the close correlation between our theoretical results and experimental observations, it appears as though a fissioning nucleus may "feel out" its potential energy surface, following rather closely a minimum potential energy path toward scission. Alternatively, the motion may be more rapid, and the mass parameter may be smoothly and slowly varying as a function of the shape variables, so that the structure of the potential surface still essentially determines the fission path. The early formation of the fragment shells is expected to lead to a collective mass parameter for the separation degree of freedom which approaches the reduced mass of the fragments soon after the second saddle; thus dynamic effects should have only little influence on our conclusions drawn from static saddle and scission point properties.

Although the dynamic calculations and solution of the complete Hamiltonian remain essential, it appears at present that the potential surface plays the dominant role. This provisional conclusion is based on the discussion of possible dynamic effects (see above), on the correlations between observed and calculated preferred mass ratios as discussed above, and on a number of previous works in which fragment deformations and total kinetic energies in low-excitation fission have been systematized on the basis of simple static-scission models.[26]

Many experiments and correlations of data over an extended period of time have pointed out the importance of fragment structure effects in fission observables. In our earlier calculations,[3] and again here, we have shown that fragment structure effects can be identified in the potential surface, and we have indicated how these develop. In the results reported here, quantitative agreement is found between the potential energy predictions near scission and the observed most probable mass divisions for a variety of nuclei.

ACKNOWLEDGMENTS

The authors gratefully acknowledge helpful and stimulating discussions with Professor W. Greiner. They are pleased to acknowledge the assistance of M. A. Stephens in carrying out the calculations.

APPENDIX A

The parameters ξ_i and α_i appearing in the single-particle potential can be determined with the help of the following conditions: (1) The nuclear shape $[\rho(z)]$ and its derivative $[\rho'(z)]$ must be continuous at $z=0$. The nuclear neck should be located at $z=0$, implying $\rho'(z=0)=0$; (2) the single-particle potential $V(\rho, z)$ and its final derivatives should be continuous at $z=0$. Conditions (1) and (2) lead to the following constraints on the potential parameters:

$$\xi_i = -\frac{1}{2z_i^2}\,, \qquad i=1,2\,, \tag{A1}$$

$$\omega_{z1}z_1 = \omega_{z2}z_2\,, \tag{A2}$$

$$\mathring{\omega}_{\rho 1}{}^2 + \tfrac{1}{2}\alpha_1 z_1{}^2 = \mathring{\omega}_{\rho 2}{}^2 + \tfrac{1}{2}\alpha_2 z_2{}^2\,. \tag{A3}$$

These four conditions together with the volume conservation constraint leave us with five independent potential parameters. Another constraint follows from the requirement that the function $\omega_{\rho i}(z)$ should be practically constant over the whole volume of the fragment nuclei when the nuclear

configuration consists of two well separated fragments. In other words, the model should be able to describe two separated Nilsson models. This condition of a very slowly varying $\omega_{\rho i}(z)$ over the fragment volume implies that α_i should decrease with increasing z_i. In order to determine this dependence we require:

$$\omega_{\rho i}^2(z=0)=\tfrac{1}{2}(\omega_{\rho 1}^2+\omega_{\rho 2}^2). \tag{A4}$$

This leads to:

$$\alpha_1=\frac{1}{z_1^2}(\mathring{\omega}_{\rho 1}^2-\mathring{\omega}_{\rho 2}^2),$$
$$\alpha_2=\frac{1}{z_2^2}(\mathring{\omega}_{\rho 1}^2-\mathring{\omega}_{\rho 2}^2). \tag{A5}$$

This additional condition then leaves us with four independent potential parameters which can be converted into shape parameters by using Eq. (4); then

$$c_i=\frac{\omega_0}{\omega_{zi}}R, \qquad a_i=\frac{\omega_0}{\mathring{\omega}_{\rho i}}R. \tag{A6}$$

Instead of these, however, we choose as shape parameters, for presentation and discussion of results, the physically more meaningful quantities $D \equiv$ radius of the neck in fermis and $\lambda \equiv$ volume ratio of the nuclear parts on either side of the neck plane. Note $\lambda=\int_{z<0}\rho\,d\rho dz/\int_{z>0}\rho\,d\rho dz$, where the integrations are to be extended over indicated parts of the nuclear volume. ($\lambda=1$ corresponds to symmetry.) The remaining two shape parameters in this framework are then:

$$\alpha=\frac{a_2}{a_1}-1,$$
$$\sigma=\frac{z_1}{\sqrt{2}\,c_1}.$$

---

*On leave from the Atomic Energy Center, Dacca, Bangladesh.

†Operated by Union Carbide Corporation for the U. S. Atomic Energy Commission.

‡Present address: Institut für Theoretische Physik, Universität Giessen, Giessen, Germany.

§Work partly supported by the U. S. Atomic Energy Commission.

[1]V. M. Strutinsky, Nucl. Phys. A95, 420 (1967); A122, 1 (1968); W. D. Myers and W. J. Swiatecki, Arkiv Fysik 36, 343 (1967).

[2]S. G. Nilsson, C. F. Tsang, A. Sobiczewski, Z. Szymanski, S. Wycech, C. Gustafson, I. L. Lamm, P. Möller and B. Nilsson, Nucl. Phys. A131, 1 (1969); M. Bolsterli, E. O. Fiset, J. R. Nix, and J. L. Norton, Phys. Rev. C 5, 1050 (1972); H. C. Pauli and T. Ledergerber, Nucl. Phys. A175, 545 (1971); V. M. Strutinsky and H. C. Pauli, in *Proceedings of the Second International Atomic Energy Symposium on Physics and Chemistry of Fission, Vienna, Austria, 1969* (International Atomic Energy Agency, Vienna, Austria, 1969), p. 155.

[3]U. Mosel and H. W. Schmitt, Nucl. Phys. A165, 73 (1971); Phys. Rev. C 4, 2185 (1971).

[4]P. Möller and S. G. Nilsson, Phys. Letters 31B, 283 (1970); V. V. Pashkevich, Nucl. Phys. A169, 275 (1971).

[5]P. Holzer, U. Mosel, and W. Greiner, Nucl. Phys. A138, 241 (1969); D. Scharnweber, W. Greiner, and U. Mosel, Nucl. Phys. A164, 257 (1971).

[6]A short note on these calculations has previously been published by M. G. Mustafa, U. Mosel, and H. W. Schmitt, Phys. Rev. Letters 28, 1536 (1972).

[7]C. Y. Wong, Phys. Letters 30B, 61 (1969); G. D. Adeev, P. A. Cherdantsev, and I. A. Gamalya, Phys. Letters 35B, 125 (1971).

[8]U. Mosel, J. Maruhn, and W. Greiner, Phys. Letters 35B, 125 (1971).

[9]A. similar generalization, with a different shape parametrization, is presently being developed by J. Maruhn and W. Greiner, Z. Physik 251, 431 (1972).

[10]D. A. Arseniev, A. Sobiczewski, and V. G. Soloviev, Nucl. Phys. A139, 269 (1969).

[11]C. Gustafson, I. L. Lamm, B. Nilsson, and S. G. Nilsson, Arkiv Fysik 36, 613 (1967).

[12]P. A. Seeger, CERN Report No. CERN 70-30, 1970 (unpublished).

[13]T. Johansson, S. G. Nilsson, and Z. Szymanski, Ann. Phys. (Paris) 5, 377 (1970).

[14]U. Mosel, Phys. Rev. C 6, 971 (1972).

[15]This is not the case in the calculations of Bolsterli *et al.* (Ref. 2) where only a one-dimensional cut into the asymmetric degree of freedom at the symmetric saddle has been calculated. At least a two-dimensional calculation is necessary to determine the saddle point.

[16]If the ground state of ^{236}U has a hexadecapole deformation, as indicated in recent Coulomb excitation experiments at this Laboratory [F. K. McGowan, C. E. Bemis, Jr., J. L. C. Ford, Jr., W. T. Milner, R. L. Robinson, and P. H. Stelson, Phys. Rev. Letters 27, 1741 (1971)], then the location of the ground state would be moved to a higher value of D; the surface around and beyond the second minimum would not be affected.

[17]H. W. Schmitt, J. H. Neiler, and F. J. Walter, Phys. Rev. 141, 1146 (1966), and references therein.

[18]N. L. Lark, G. Sletten, J. Pedersen, and S. Bjørnholm, Nucl. Phys. A139, 481 (1969).

[19]R. Brandt, S. G. Thompson, R. C. Gatti, and L. Phillips, Phys. Rev. 131, 2617 (1963).

[20]K. F. Flynn, E. P. Horwitz, C. A. A. Bloomquist, R. F. Barnes, R. K. Sjoblom, P. R. Fields, and L. E. Glendenin, Phys. Rev. C 5, 1725 (1972).

[21]W. John, E. K. Hulet, R. W. Lougheed, and J. J. Wesolowski, Phys. Rev. Letters 27, 45 (1971).

[22]J. P. Balagna, G. P. Ford, D. C. Hoffman, and J. D. Knight, Phys. Rev. Letters 26, 145 (1971).

[23]J. R. Nix, W. J. Swiatecki, Nucl. Phys. 71, 1 (1965); J. R. Nix, Nucl. Phys. A130, 241 (1969).

[24]F. Plasil, D. S. Burnett, H. C. Britt, and S. G. Thompson, Phys. Rev. 142, 696 (1966).

[25]L. G. Moretto, S. G. Thompson, J. Routti, and R. C. Gatti, Phys. Letters 38B, 471 (1972).
[26]See, e.g., H. W. Schmitt, in *Proceedings of the Second International Atomic Energy Symposium on Physics and Chemistry of Fission, Vienna, Austria, 1969* (see Ref. 2), p. 67, and references therein; also H. W. Schmitt and U. Mosel, Nucl. Phys. A186, 1 (1972).

PHYSICAL REVIEW C VOLUME 7, NUMBER 4 APRIL 1973

Neutron Resonance Parameters of ^{92}Mo†

O. A. Wasson
Brookhaven National Laboratory, Upton, New York 11973, and Oak Ridge National Laboratory, Oak Ridge, Tennessee 37830

and

B. J. Allen
Australian Atomic Energy Commission, Lucas Heights, Australia, and Oak Ridge National Laboratory, Oak Ridge, Tennessee 37830

and

R. R. Winters
Denison University, Granville, Ohio 43023, and Oak Ridge National Laboratory, Oak Ridge, Tennessee 37830

and

R. L. Macklin and J. A. Harvey
Oak Ridge National Laboratory, Oak Ridge, Tennessee 37830

(Received 21 August 1972)

Neutron transmission and total neutron-capture yields were measured using the time-of-flight technique at the Oak Ridge electron linear accelerator facility using enriched samples of ^{92}Mo. A total of 42 resonances were observed for neutron energies less than 32 keV. 12 are assigned to s-wave interactions, while 23 are assigned to p-wave interactions. The resonant energies, neutron widths, radiation widths, and spins are deduced. The average s- and p-wave radiation widths are equal to 0.178 ± 0.015 eV and 0.24 ± 0.03 eV, respectively. The s-wave neutron strength function is $(0.65 \pm 0.26) \times 10^{-4}$, while the p-wave strength function is $(3.3 \pm 1.1) \times 10^{-4}$.

I. INTRODUCTION

A recent development in the field of radiative neutron capture is the observation of the importance of single-particle or valency contribution to the γ-ray decay of the neutron resonances for nuclei near the peak of the $3p$ neutron strength function.[1-4] In a separate paper[5] capture γ-ray spectral measurements are reported for resonant neutron capture in the target nucleus ^{92}Mo for neutron energies less than 25 keV. One purpose of the present paper is to supply the neutron resonance parameters required to calculate the valency model contributions to the γ-ray transition probabilities for this nucleus. Previous measurements[6] of the total neutron cross section, which employed samples of natural isotopic composition, identified only a few resonances in ^{92}Mo. Total neutron-capture measurements by Weigman, Rohr, and Winter[7] using enriched samples were limited to neutron energies less than 10 keV.

The present work reports the results of neutron transmission and total neutron-capture experiments performed at the Oak Ridge electron linear accelerator (ORELA). Neutron resonance parameters for the target nucleus ^{92}Mo are deduced for neutron energies less than 32 keV where only s- and p-wave neutron interactions are significant. The required parameters are the neutron width Γ_n, the total radiation width Γ_γ, and the spin and parity of the resonance J^π_λ.

The parities of the resonances are determined from the shapes of the transmission dips. The s-wave resonances are identified by the asymmet-